PHYSICS

Toward tailoring Majorana bound states in artificially constructed magnetic atom chains on elemental superconductors

Howon Kim,[1]* Alexandra Palacio-Morales,[1] Thore Posske,[1] Levente Rózsa,[1] Krisztián Palotás,[2,3] László Szunyogh,[4] Michael Thorwart,[1] Roland Wiesendanger[1]*

Realizing Majorana bound states (MBS) in condensed matter systems is a key challenge on the way toward topological quantum computing. As a promising platform, one-dimensional magnetic chains on conventional superconductors were theoretically predicted to host MBS at the chain ends. We demonstrate a novel approach to design of model-type atomic-scale systems for studying MBS using single-atom manipulation techniques. Our artificially constructed atomic Fe chains on a Re surface exhibit spin spiral states and a remarkable enhancement of the local density of states at zero energy being strongly localized at the chain ends. Moreover, the zero-energy modes at the chain ends are shown to emerge and become stabilized with increasing chain length. Tight-binding model calculations based on parameters obtained from ab initio calculations corroborate that the system resides in the topological phase. Our work opens new pathways to design MBS in atomic-scale hybrid structures as a basis for fault-tolerant topological quantum computing.

INTRODUCTION

Majorana fermions (*1*)—particles being their own antiparticles—have recently attracted renewed interest in various fields of physics. In condensed matter systems, Majorana bound states (MBS) with a non-Abelian quantum exchange statistics have been proposed as a key element for topological quantum computing (*2*–*4*). One of the most promising platforms to realize MBS are one-dimensional (1D) helical spin systems being proximity-coupled to a conventional s-wave superconductor (*5*–*9*). In such a surface-confined system, the MBS can directly be investigated by local probe techniques such as scanning tunneling microscopy/spectroscopy (STM/STS). Previously reported experiments aiming at the direct visualization and probing of the MBS have focused on self-assembled magnetic chains on superconducting Pb substrates (*10*–*15*). However, such self-assembled nanowires have unavoidable limitations, for example, a lack of control over chain structure and length, as well as problems with atomic intermixing between the magnetic adsorbates and the Pb substrate during the annealing process, which is required to form the 1D chains. The unclear geometric and electronic structure of the magnetic nanowires can lead to ambiguous interpretations and make them inadequate to serve as true model systems for MBS (*16*–*18*).

Here, we demonstrate the atomically controlled fabrication of 1D Fe chains on a superconducting Re(0001) substrate using STM-based single-atom manipulation methods (*19*). The precise positioning of individual Fe atoms, together with the local probing of the local density of states (LDOS) around the Fermi energy by STS, makes it possible to build up atomic chains of controlled length without any ambiguities concerning the geometric and electronic structure of the chains.

[1]Department of Physics, University of Hamburg, D-20355 Hamburg, Germany. [2]Institute of Physics, Slovak Academy of Sciences, 84511 Bratislava, Slovakia. [3]MTA-SZTE Reaction Kinetics and Surface Chemistry Research Group, University of Szeged, 6720 Szeged, Hungary. [4]Department of Theoretical Physics and MTA-BME Condensed Matter Research Group, Budapest University of Technology and Economics, 1111 Budapest, Hungary.
*Corresponding author. Email: hkim@physnet.uni-hamburg.de (H.K.); wiesendanger@physnet.uni-hamburg.de (R.W.)

RESULTS

As a building block for the atomic chains, we first explored the electronic structure of individual Fe atoms. Figure 1 shows STM/STS data of single Fe atoms (Fig. 1A) and an Fe dimer (Fig. 1B), which were positioned to specific sites by STM-based single-atom manipulations (Materials and Methods). The Fe atoms with localized magnetic moments can be distinguished from nonmagnetic adsorbates by identifying the so-called Yu-Shiba-Rusinov (YSR) bound states (*20*–*22*), which are reflecting the quasi-particle excitations of the broken Cooper pair on the superconducting surface. The YSR states of the magnetic Fe atoms show up as a pair of characteristic resonances inside the superconducting gap of Re (Δ_{Re} = 0.28 meV) around the Fermi energy in differential tunneling conductance (dI/dV) spectra (*23*–*25*) displayed in Fig. 1C, which are a direct probe of the system's LDOS. The pair of resonances lie very close to the Fermi level (~±0.020 meV), so at the experimental temperature (350 mK or 0.030 meV), they could only be resolved by a superconducting Nb tip (Fig. 1C), but not with the non-superconducting PtIr tip because of the thermal broadening (red curves in Fig. 1, D and E).

When a dimer is formed from two Fe atoms at neighboring hexagonal close-packed (hcp) hollow sites on the Re(0001) substrate at a distance of a_{Re} = 0.274 nm (Fig. 1B), they become strongly coupled and form hybridized YSR states. In Fig. 1 (D and E), these hybridized states appear as broad resonances with peaks or shoulders located at ~±0.110 meV and pronounced asymmetric spectral weights compared to the ones for single Fe adatoms (see also fig. S1 for spatial distributions) (*26*). This hybridization of the YSR states between the magnetic adatoms is a requirement for the formation of MBS in the chains discussed below.

Subsequently, we fabricated 1D atomic chains by placing Fe atoms in hcp hollow sites along one of the close-packed directions ([1$\bar{1}$0]) of the Re crystal, as schematically depicted in Fig. 2A, making use of STM-based atom-by-atom manipulations (Materials and Methods). Figure 2B shows intermediate steps of creating the chain starting from a dimer and ending with a length of 40 atoms (see also movie S1). Before attaching them to the chain, each individual Fe atom was identified by confirming the characteristic YSR bound state energies in the dI/dV

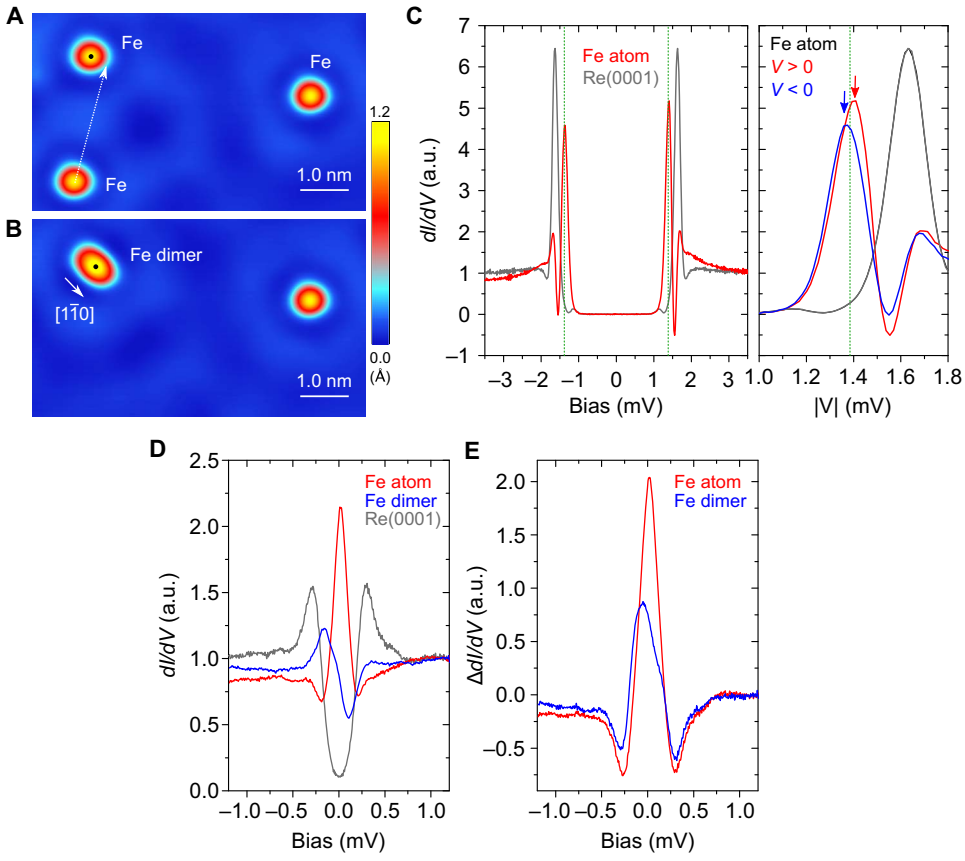

Fig. 1. YSR states of individual magnetic Fe atoms and their interactions on Re(0001). (**A** and **B**) STM topographic images of isolated Fe atoms (A) and an Fe dimer (B) on Re(0001). Tunneling current, I_T = 5.0 nA; sample bias voltage, V_S = 3.0 mV; scan area, 7.0 × 4.0 nm^2. The Fe dimer in (B) was created by placing an Fe atom next to another [white dotted arrow in (A)] at a distance of a_{Re} = 0.274 nm. (**C**) Left: *dI*/*dV* spectra on a single Fe atom (red) and on the bare Re substrate (gray) measured with a superconducting Nb tip (I_T = 1.0 nA, V_S = 3.0 mV). Right: Same spectra plotted as a function of |*V*|. The green dotted line indicates the energy position of the superconducting gap edge of the Nb tip (Materials and Methods). A pair of YSR resonances are indicated by red and blue arrows at $|\Delta_{Nb} \pm E_B|$, with Δ_{Nb} = 1.38 meV and E_B = 0.020 meV, providing a signature for the localized magnetic moment of the Fe atom. (**D**) *dI*/*dV* spectra obtained at the positions marked by black dots in (A) and (B) for a single Fe atom (red), an Fe dimer (blue), and the bare Re(0001) (gray) measured with a nonsuperconducting tip (I_T=5.0 nA, V_S=1.5 mV). (**E**) Difference spectra for an Fe atom and a dimer after subtracting the spectrum obtained on the bare Re(0001) surface. Except for (C), a PtIr tip was used for taking topography images and spectra. All STM images and tunneling spectra were measured at *T* = 350 mK. a.u., arbitrary units.

spectra shown in Fig. 1. The smooth and uniform STM topography images in Fig. 2 (B and C) indicate the well-defined atomic structure of the constructed chains.

To understand the magnetic structure of atomic Fe chains on Re(0001), we performed spin-polarized STM (SP-STM) measurements with Fe-coated PtIr tips (*27*, *28*), which are sensitive to the direction of the localized magnetic moments on the surface with respect to the tip magnetization direction (Materials and Methods) (*28*). The SP-STM images obtained with different magnetic tips being sensitive to either the out-of-plane (OP) or in-plane (IP) spin components (Fig. 2, D and E, respectively) show clear spatial modulations along the chain with periods of ~0.36 nm ($4/3a_{Re}$) and ~1.1 nm ($4a_{Re}$) (see also the bottom part of Fig. 3A and fig. S2 for the real-space profile and the fast Fourier transform analysis). Because the STM image in Fig. 2C obtained with a nonmagnetic probe tip shows a featureless surface profile, these modulations can be attributed to the magnetic structure. Furthermore, the shifted phase of the spatial oscillations between SP-STM images recorded with differently oriented magnetic tips proves the presence of a spin spiral ground state (*29*) for the Fe chain on Re(0001), which was theoretically assumed for the prediction of MBS at chain ends (*5*–*9*). The spin spiral ground state originates from interfacial Dzyaloshinsky-Moriya interaction, which is strong for Fe chains on 5d transition metal substrates (*29*). This is in stark contrast to the cases of self-assembled Fe and Co chains on Pb(110), which were reported to be ferromagnetic (*10*, *14*).

A typical characteristic of MBS is an enhancement of the LDOS spatially localized at the ends of the chain and at zero energy (*10*–*13*, *15*). To explore this property for the 40-atom-long Fe chain, we measured spatially resolved *dI*/*dV* spectra along the chain. Figure 3A displays the spatial variation of the LDOS by plotting the difference between the *dI*/*dV* values measured on the chain and on the substrate at four different bias voltages: *V* = 0.00 mV (zero energy), ±0.12 mV (inside the gap), and −0.65 mV (outside the gap). Note that the LDOS profiles at ±0.12 mV have been chosen to reveal the spatial modulation of the hybridized YSR states in the chain. We find that the measured *dI*/*dV* profiles at zero energy indicate an enhancement of the LDOS with the highest peaks at both ends of the chain (red and orange arrows in Fig. 3A). Although the profiles at +0.12 mV also display enhancements at the ends of the chain, the enhancement of the zero-energy LDOS is localized half a lattice constant of Re(0001) away from the one at +0.12 mV (Fig. 3, A and C).

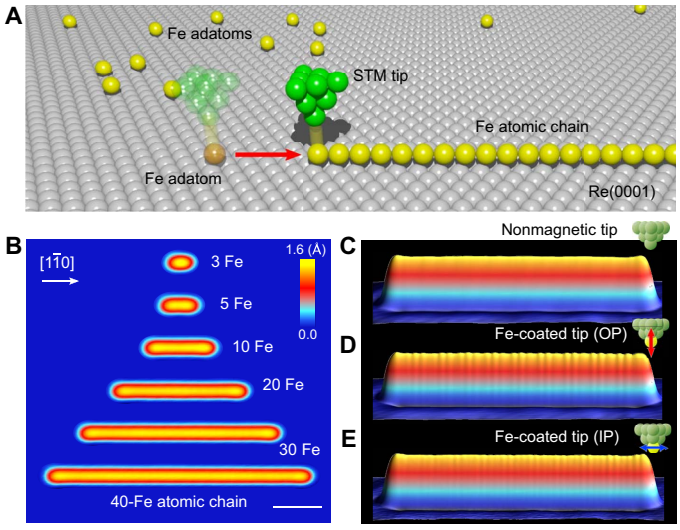

Fig. 2. Artificially constructed atomic Fe chains on Re(0001) and SP-STM measurements for the magnetic structure. (**A**) Schematic view of the atom manipulation procedure applied to form a 1D atomic chain with an STM tip. (**B**) Stacked STM images for the artificially constructed Fe chains of various lengths along the close-packed [1$\bar{1}$0] direction (I_T = 5.0 nA, V_S = 3.0 mV; scale bar, 2.0 nm). (**C**) 3D-rendered STM image of a 40-atom-long Fe chain measured with a nonmagnetic PtIr tip. (**D** and **E**) SP-STM images recorded with Fe-coated PtIr tips sensitive to the (D) OP and the (E) IP component of the spins in the chain, with the magnetization directions schematically depicted in the inset. The same tunneling conditions of I_T = 5.0 nA and V_S = 3.0 mV were used for the measurements in (C) to (E). The magnetization directions of the Fe-coated tips were determined in situ directly before the SP-STM measurements on the atomic Fe chains (Materials and Methods) (*28*).

The *dI*/*dV* spectra obtained on the chain in Fig. 3B display an enhanced and considerably asymmetric LDOS inside the gap, which can be attributed to the hybridized YSR states. At the chain ends (red and orange curves), we observe shoulders in the spectra around zero energy, contributing to the highest peaks in the spatially resolved profile (Fig. 3A), whereas these shoulders are absent in the spectra at the middle of the chain (green and blue curves). However, it is difficult to unambiguously separate the contributions to these shoulders from the YSR states and from a possible MBS inside a topological superconducting gap in the *dI*/*dV* spectra because of the limited energy resolution at the current experimental temperature (~350 mK).

Note that electron confinement effects not connected to superconductivity are also observed in the 1D chain, however, at energies outside the gap (−0.65 meV, dark cyan curve in Fig. 3A). Moreover, the spatial positions of the peaks (dark cyan arrows) outside the gap are significantly different from the ones at zero energy. On the other hand, all subgap features disappear above the superconducting transition temperature (T_C ~ 1.6 K) of the Re substrate (see fig. S3 and movie S3). This proves that the observed in-gap features of the 1D magnetic chain are strongly linked to the superconductivity of the Re substrate.

Most remarkably, the overall *dI*/*dV* profiles in Fig. 3A exhibit a symmetric distribution of the LDOS with respect to the center of the chain, as it should be for an ideal chain composed of regularly arranged Fe atoms without any geometric or chemical defects. In addition, the periodic modulations of the zero-energy LDOS show a clear correlation with the periodicity in the SP-STM profile, which are significantly different from the previously studied self-assembled Fe chains on the Pb substrate with inhomogeneous LDOS (*10*–*13*, *15*). The enhanced LDOS at zero energy at the ends of the chain is visualized in the spatially and energy-resolved tunneling conductance maps in Fig. 3C (see also movie S2), also displaying the symmetry between the two ends.

To gain more insight into the nature of the observed enhanced LDOS at zero energy at the chain ends, we explored the spatial distribution of the LDOS for atomic chains of various lengths. Figure 4A shows *dI*/*dV* profiles at zero energy along close-packed chains consisting of 3 to 12, 20, 30, and 40 Fe atoms. The measured profiles for most chains show a symmetric distribution with respect to the center and exhibit strong spatial modulations within the chains because of the formation of the hybridized YSR states. For shorter chains, the values of zero-energy conductance measured both at the ends and in the middle oscillate as the number of atoms in the chain is increased. However, for longer chains, a considerable difference develops between the LDOS values measured at the ends and in the middle, also shown in Fig. 4B. Both the conductance values (Fig. 4B) and the shape of the LDOS profiles (Figs. 3A and 4A) at the ends of the chains gradually become stabilized with increasing chain lengths at around 12 atoms. These observations indicate that a minimum number of Fe atoms are necessary to fully develop a spatially localized electronic state at the chain ends around the Fermi energy.

To further elucidate the nature of the experimentally observed localization of the enhanced zero-energy LDOS at the chain ends, we examined a realistic nearest-neighbor tight-binding model describing the atomic Fe chain in the experimentally determined spin spiral state (Fig. 2, D and E). As shown in Fig. 4C, we found that the chain with noncollinear spin structure resides in a topologically nontrivial phase in a wide parameter range, where MBS are expected to be formed. By using material-specific parameters for the Fe chain on Re(0001) derived from first-principles calculations (sections S1 and S2, and Supplementary Materials), the theoretical model suggests that the current system is in the topologically nontrivial superconducting phase.

Finally, it is worth mentioning that our detailed studies on artificially constructed atomic Fe chains on Re(0001) have shown that local structural or chemical defects can significantly modify the LDOS at the ends of the chains, for example, zero-bias peaks at the chain end can be generated by single-atom defects. In Fig. 5, we constructed an 8-atom-long Fe chain with a single structural defect at one end of the chain, which shows an asymmetric apparent height in the surface profile (Fig. 5F). The defect-free 8-atom-long chain displays a quite flat spatial modulation of the zero-energy LDOS in the bottom part of Fig. 5G, which cannot be interpreted as an indication for the presence of an MBS (see also Fig. 4, A and B). Surprisingly, although it is expected not to observe an enhancement of the zero-energy LDOS at the ends of the perfect 8-atom-long Fe chain (Fig. 4, A and B), such a structural defect creates a localized defect state at the Fermi energy in the spectroscopic maps, as shown in Fig. 5G, which is absent at the other end and for the defect-free 8-atom-long chain. This implies that single-atom control, as demonstrated by our experiments, is required to safely rule out defect-induced zero-energy modes mimicking MBS at the chain ends.

DISCUSSION

In conclusion, we have demonstrated that single-atom manipulation techniques offer a reliable and unique pathway to design and realize model-type platforms with well-defined atomic, electronic, and magnetic structures. We investigated signatures of MBS by performing STS measurements

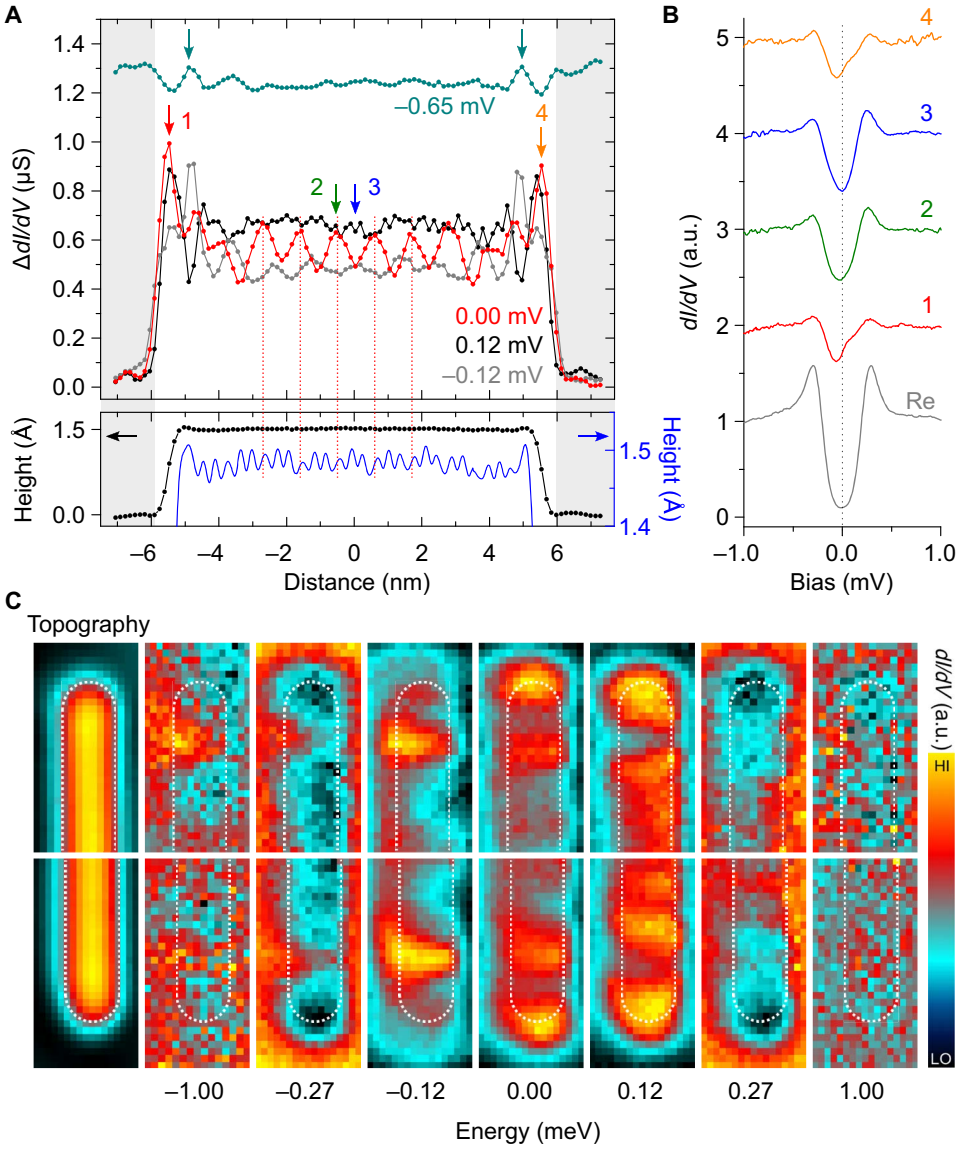

Fig. 3. Spatial and energy dependence of the LDOS in the 40-atom-long chain. (**A**) Top: Differential tunneling conductance (*dI*/*dV*) profiles at V_S = 0.00 mV, +0.12 mV, −0.12 mV, and −0.65 mV along the 40-atom-long Fe chain, reflecting the spatial variation of the LDOS. All profiles were extracted from the spatially resolved *dI*/*dV* spectra after subtracting the spectrum on the bare Re substrate. The profile for V = −0.65 mV is vertically shifted for clarity (offset, 1.3 μS). Dark cyan arrows in the profile at −0.65 mV denote spatial locations for the confined states; the other colors show the spatial positions where the energy-resolved spectra in (B) were measured. Bottom: Constant-current STM profile (black, left vertical axis), which was recorded simultaneously with the *dI*/*dV* spectra and corresponding magnetic profile (blue, right vertical axis) obtained from the SP-STM image measured with the OP spin-sensitive tip. The gray shaded regions correspond to the Re substrate. The dotted lines in red are guides to the eye for the comparison of the spatial variation of the LDOS with the SP-STM profile. (**B**) *dI*/*dV* spectra obtained at the positions indicated by the arrows in (A) and the gray one for the Re substrate. The dotted vertical line shows the zero energy. (**C**) Spatial distribution of the LDOS at various energies for the two different ends of the 40-atom-long Fe chain. The white dotted lines indicate the boundary of the chain. The scan size of all images is 1.1 nm × 2.2 nm. The intensity scale at the right side is adjusted for each figure separately. Both ends show an identical and symmetric distribution of LDOS with respect to the center of the chain. The localized end states are visible in the LDOS maps at zero energy for both ends. The tunnel junctions were stabilized at I_T = 5.0 nA and V_S = 3.0 mV for all spectroscopic measurements.

and found an enhancement in the zero-energy LDOS localized at the chain ends. Theoretical calculations confirm that the Fe chain on the Re substrate is in the topological superconducting phase. From the experimental point of view, improving the energy resolution at lower temperature or investigating the spin-polarized nature of in-gap states in future experimental studies will allow a more direct access to the topological character of the chains (*15*, *30*). However, most importantly, the methodology introduced in this study can straightforwardly be extended to more complex magnetic adatom structures on various superconducting substrates, going far beyond linear adatom arrangements. This new approach will pave the way not only for a deeper fundamental insight into the underlying physics of MBS but also for their future applications in topological quantum computing (*2*–*4*, *31*).

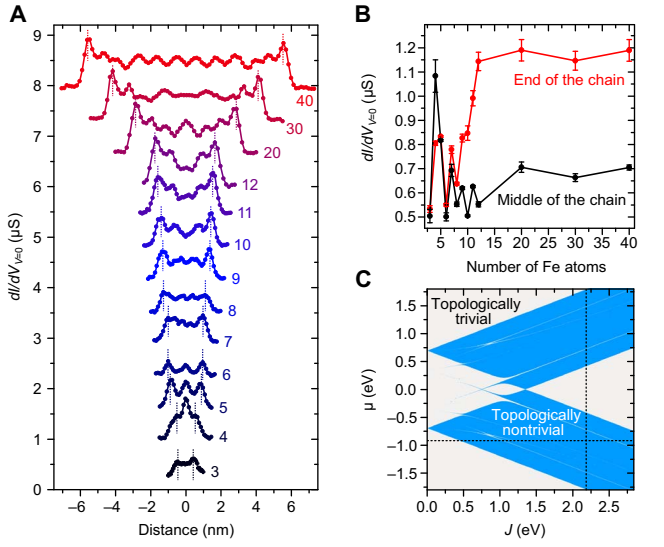

Fig. 4. Development and stabilization of enhanced zero-energy LDOS at the ends with increasing chain length and the calculated topological phase diagram for the Fe chain. (**A**) Measured zero-energy *dI*/*dV* profiles along the chains for (from bottom to the top) 3 to 12, 20, 30, and 40 Fe atoms. For clarity, the profiles are shifted vertically. (**B**) Comparison of the variation of zero-energy tunneling conductance between the middle and the ends of the chains with increasing number of atoms. The conductance values at the end are averaged over the positions indicated by the two dotted lines in the profiles, whereas the ones for the middle are averaged values from the regions around the center of the chains. The tunneling junctions were stabilized at I_T = 5.0 nA and V_S = 3.0 mV for all spectroscopic measurements. (**C**) Calculated topological phase diagram for a straight monoatomic Fe chain with noncollinear magnetization as a function of the on-site energy μ and spin splitting parameter *J* (section S3 and Supplementary Materials). Blue and gray shaded regions correspond to the topologically nontrivial superconducting phase and the trivial phase, respectively. The two dotted lines represent the parameters determined from ab initio calculations for Fe on the Re(0001) surface, μ = −0.92 eV and *J* = 2.18 eV.

MATERIALS AND METHODS

Preparation of the sample and the tip

The rhenium single crystal was prepared by repeated cycles of O_2 annealing at 1400 K followed by flashing at 1800 K to obtain an atomically flat Re(0001) surface (*28*, *32*). Fe was deposited with a 0.6 to 0.7 monolayer (ML) coverage onto the clean Re(0001) surface in situ at room temperature from a pure Fe rod (99.99+%) using an electron beam evaporator. The surface cleanliness was checked by STM after transferring the sample into the cryostat. For most measurements, we used a mechanically polished Pt/Ir alloy wire as the STM tip. The tip was conditioned by applying voltage pulses (about a few volts for 50 ms), and its quality was judged to be suitable if it showed a flat LDOS outside the superconducting gap of rhenium. A mechanically cut Nb wire was used as a superconducting tip to improve the energy resolution in the tunneling spectra for the Fe adatom on Re.

STM/STS and SP-STM measurements

All the experiments were carried out in a ^{3}He-cooled low-temperature STM system (USM-1300S, Unisoku, Japan) operating at T = 350 mK under ultrahigh vacuum conditions. Tunneling spectra were obtained by measuring the differential tunneling conductance (*dI*/*dV*) using a standard lock-in technique with a modulation bias voltage of 20 μV and a frequency of 971 Hz with opened feedback loop. The bias voltage was applied to the sample, and the tunneling current was measured through the tip using a commercially available controller (Nanonis, SPECS, Swiss). For STS measurements with the Nb tip, we estimated the energy position of the superconducting gap edge of the tip (green dotted lines in Fig. 1C) from the tunneling spectrum on the Re substrate. Note that the two pairs of peaks in the spectrum on Re correspond to $\pm|\Delta_{Re} - \Delta_{Nb}|$ and $\pm|\Delta_{Re} + \Delta_{Nb}|$, respectively ($\Delta_{Re}$ = 0.28 meV, Δ_{Nb} = 1.38 meV) (*33*–*35*). For SP-STM measurements, we coated several Fe atoms in situ at the apex of PtIr tips by picking them up from an Fe island. The magnetization directions of the Fe-coated tip were determined by revealing the

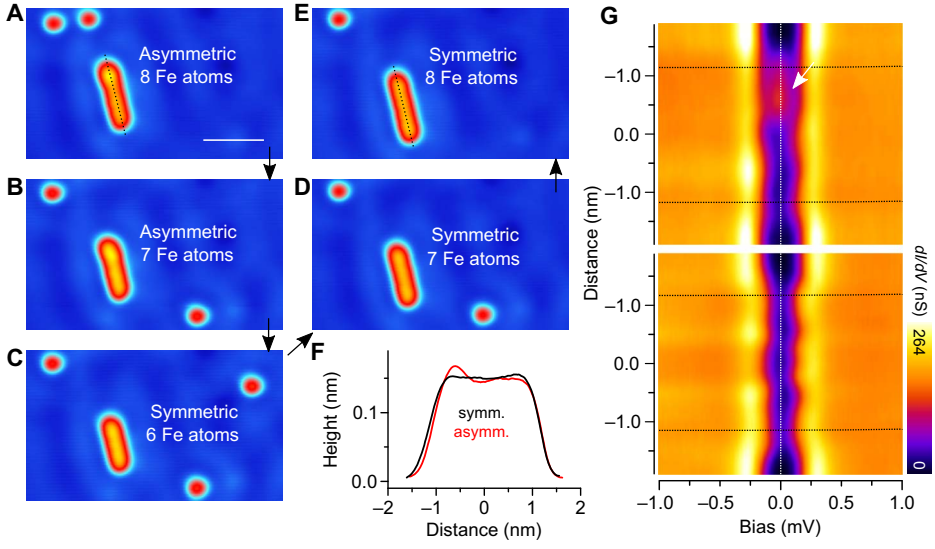

Fig. 5. Defect-induced zero-energy in-gap state for an Fe chain with a structural defect. (**A** to **E**) Sequential STM images for the demonstration of disassembling (A to C) and reassembling (C to E) the 8-atom-long Fe chain by continuous atom manipulations (scale bar, 2.0 nm). (**F**) Surface profiles along the dotted lines in (A) and (E) for the asymmetric and symmetric 8-atom-long chain, respectively. The 8- and 7-atom-long Fe chains in (A) and (B) show an asymmetric apparent height and are slightly bent from the chain axis because of the mislocated Fe atoms in the chains. After reassembling the 8-atom-long Fe chain, it becomes symmetric and straight. (**G**) Spatially resolved *dI*/*dV* spectra and the color-encoded spectroscopic maps for the asymmetric (top) and symmetric (bottom) 8-atom-long Fe chains. The black dotted lines indicate the boundary between the chains and the substrate. The white arrow indicates the defect-induced zero-energy bound state, which is absent at the other end and at the ends of the symmetric chain. We stabilized the tunneling junction at I_T = 5.0 nA and V_S = 3.0 mV for all STM images and the tunneling spectra.

magnetic contrast of spin spirals in ML-thick Fe islands on Re(0001), as discussed in detail by Palacio-Morales *et al.* (*28*).

Vertical and lateral STM tip–induced atom manipulation

Single Fe atoms were introduced by a vertical manipulation method from ML-thick Fe islands on the Re(0001) surface (*36*). The STM tip was softly indented into the Fe islands to pick up several Fe atoms and release them onto the clean Re(0001) surface by adjusting the tip-sample distance. Fe atoms were identified after vertical transfer by observing the characteristic YSR states of single Fe atoms on Re(0001) in the tunneling spectra. Nonmagnetic atoms, which are mostly from the tip materials and sometimes also transferred to the surface during the vertical atom manipulation process, do not exhibit YSR states. We applied the lateral atom manipulation method to form Fe atomic chains. We switched the tunneling parameters from imaging condition (2.0 to 5.0 nA, 3.0 mV) to manipulation condition (90 to 120 nA, 3.0 mV) after placing the tip next to a single Fe atom. We picked up an atom by moving the tip across it and manipulated the Fe atom precisely to the aimed atomic site of the Re(0001) surface with closed feedback loop while monitoring the profile of the tip movement. STM images after sequential atom manipulations were collected during the formation of the Fe chains (see movie S1).

SUPPLEMENTARY MATERIALS

Supplementary material for this article is available at http://advances.sciencemag.org/cgi/content/full/4/5/eaar5251/DC1

section S1. Ab initio calculations

section S2. Model parameters

section S3. Tight-binding model

fig. S1. Spatial distribution of the YSR states for a single Fe atom and an Fe dimer on the Re(0001) surface.

fig. S2. The fast Fourier transformation analysis for the magnetic structure of the 40-atom-long Fe chain.

fig. S3. Absence of the in-gap states on the 40-atom-long Fe chain above the superconducting critical temperature of Re.

movie S1. Demonstration of subsequent atom manipulations to construct the close-packed chains of various lengths.

movie S2. Spatially resolved 2D spectroscopic maps for two different ends of the 40-atom-long Fe chain below T_C.

movie S3. Spatially resolved 2D spectroscopic maps for the 40-atom-long Fe chain above T_C.

References (*37*–*46*)

REFERENCES AND NOTES

1. E. Majorana, Symmetrical theory of electrons and positrons. *Nuovo Cim.* **14**, 171–184 (1937).
2. C. W. J. Beenakker, Search for Majorana fermions in superconductors. *Annu. Rev. Condens. Matter Phys.* **4**, 113–136 (2011).
3. J. Alicea, New directions in the pursuit of Majorana fermions in solid state systems. *Reports Prog. Phys.* **75**, 76501 (2012).
4. S. R. Elliott, M. Franz, Colloquium : Majorana fermions in nuclear, particle, and solid-state physics. *Rev. Mod. Phys.* **87**, 137–163 (2015).
5. S. Nadj-Perge, I. K. Drozdov, B. A. Bernevig, A. Yazdani, Proposal for realizing Majorana fermions in chains of magnetic atoms on a superconductor. *Phys. Rev. B* **88**, 020407 (2013).
6. F. Pientka, L. I. Glazman, F. von Oppen, Topological superconducting phase in helical Shiba chains. *Phys. Rev. B* **88**, 155420 (2013).
7. M. M. Vazifeh, M. Franz, Self-organized topological state with Majorana fermions. *Phys. Rev. Lett.* **111**, 206802 (2013).
8. J. Klinovaja, P. Stano, A. Yazdani, D. Loss, Topological superconductivity and Majorana fermions in RKKY systems. *Phys. Rev. Lett.* **111**, 186805 (2013).
9. B. Braunecker, P. Simon, Interplay between classical magnetic moments and superconductivity in quantum one-dimensional conductors: Toward a self-sustained topological Majorana phase. *Phys. Rev. Lett.* **111**, 147202 (2013).
10. S. Nadj-Perge, I. K. Drozdov, J. Li, H. Chen, S. Jeon, J. Seo, A. H. MacDonald, B. A. Bernevig, A. Yazdani, Observation of Majorana fermions in ferromagnetic atomic chains on a superconductor. *Science* **346**, 602–607 (2014).
11. M. Ruby, F. Pientka, Y. Peng, F. von Oppen, B. W. Heinrich, K. J. Franke, End states and subgap structure in proximity-coupled chains of magnetic adatoms. *Phys. Rev. Lett.* **115**, 197204 (2015).
12. R. Pawlak, M. Kisiel, J. Klinovaja, T. Meier, S. Kawai, T. Glatzel, D. Loss, E. Meyer, Probing atomic structure and Majorana wavefunctions in mono-atomic Fe chains on superconducting Pb surface. *npj Quantum Inf.* **2**, 16035 (2016).
13. B. E. Feldman, M. T. Randeria, J. Li, S. Jeon, Y. Xie, Z. Wang, I. K. Drozdov, B. A. Bernevig, A. Yazdani, High-resolution studies of the Majorana atomic chain platform. *Nat. Phys.* **13**, 286–291 (2016).
14. M. Ruby, B. W. Heinrich, Y. Peng, F. von Oppen, K. J. Franke, Exploring a proximity-coupled Co chain on Pb(110) as a possible Majorana platform. *Nano Lett.* **17**, 4473–4477 (2017).
15. S. Jeon, Y. Xie, J. Li, Z. Wang, B. A. Bernevig, A. Yazdani, Distinguishing a Majorana zero mode using spin-resolved measurements. *Science* **358**, 772–776 (2017).
16. J. Liu, A. C. Potter, K. T. Law, P. A. Lee, Zero-bias peaks in the tunneling conductance of spin-orbit-coupled superconducting wires with and without Majorana end-states. *Phys. Rev. Lett.* **109**, 267002 (2012).
17. J. D. Sau, P. M. R. Brydon, Bound states of a ferromagnetic wire in a superconductor. *Phys. Rev. Lett.* **115**, 127003 (2015).
18. E. Dumitrescu, B. Roberts, S. Tewari, J. D. Sau, S. Das Sarma, Majorana fermions in chiral topological ferromagnetic nanowires. *Phys. Rev. B* **91**, 094505 (2015).
19. D. M. Eigler, E. K. Schweizer, Positioning single atoms with a scanning tunnelling microscope. *Nature* **344**, 524–526 (1990).
20. L. Yu, Bound state in superconductors with paramagnetic impurities. *Acta Phys. Sin.* **21**, 75–91 (1965).
21. H. Shiba, Classical spins in superconductors. *Prog. Theor. Phys.* **40**, 435–451 (1968).
22. A. I. Rusinov, On the theory of gapless superconductivity in alloys containing paramagnetic impurities. *Sov. J. Exp. Theor. Phys.* **29**, 1101 (1969).
23. A. Yazdani, B. A. Jones, C. P. Lutz, M. F. Crommie, D. M. Eigler, Probing the local effects of magnetic impurities on superconductivity. *Science* **275**, 1767–1770 (1997).
24. S.-H. Ji, T. Zhang, Y.-S. Fu, X. Chen, X.-C. Ma, J. Li, W.-H. Duan, J.-F. Jia, Q.-K. Xue, High-resolution scanning tunneling spectroscopy of magnetic impurity induced bound states in the superconducting gap of Pb thin films. *Phys. Rev. Lett.* **100**, 226801 (2008).
25. M. Ruby, F. Pientka, Y. Peng, F. von Oppen, B. W. Heinrich, K. J. Franke, Tunneling processes into localized subgap states in superconductors. *Phys. Rev. Lett.* **115**, 087001 (2015).
26. D. K. Morr, N. A. Stavropoulos, Quantum interference between impurities: Creating novel many-body states in *s*-wave superconductors. *Phys. Rev. B* **67**, 020502 (2003).
27. R. Wiesendanger, Spin mapping at the nanoscale and atomic scale. *Rev. Mod. Phys.* **81**, 1495–1550 (2009).
28. A. Palacio-Morales, A. Kubetzka, K. von Bergmann, R. Wiesendanger, Coupling of coexisting noncollinear spin states in the Fe monolayer on Re(0001). *Nano Lett.* **16**, 6252–6256 (2016).
29. M. Menzel, Y. Mokrousov, R. Wieser, J. E. Bickel, E. Vedmedenko, S. Blügel, S. Heinze, K. von Bergmann, A. Kubetzka, R. Wiesendanger, Information transfer by vector spin chirality in finite magnetic chains. *Phys. Rev. Lett.* **108**, 197204 (2012).
30. J. J. He, T. K. Ng, P. A. Lee, K. T. Law, Selective equal-spin Andreev reflections induced by Majorana fermions. *Phys. Rev. Lett.* **112**, 037001 (2014).
31. J. Li, T. Neupert, B. A. Bernevig, A. Yazdani, Manipulating Majorana zero modes on atomic rings with an external magnetic field. *Nat. Commun.* **7**, 10395 (2016).
32. S. Ouazi, T. Pohlmann, A. Kubetzka, K. von Bergmann, R. Wiesendanger, Scanning tunneling microscopy study of Fe, Co and Cr growth on Re(0001). *Surf. Sci.* **630**, 280–285 (2014).
33. M. Ternes, W.-D. Schneider, J.-C. Cuevas, C. P. Lutz, C. F. Hirjibehedin, A. J. Heinrich, Subgap structure in asymmetric superconducting tunnel junctions. *Phys. Rev. B* **74**, 132501 (2006).
34. M. Hurd, S. Datta, P. F. Bagwell, Current-voltage relation for asymmetric ballistic superconducting junctions. *Phys. Rev. B* **54**, 6557–6567 (1996).
35. M. Hurd, S. Datta, P. F. Bagwell, ac Josephson effect for asymmetric superconducting junctions. *Phys. Rev. B* **56**, 11232–11245 (1997).
36. L. Limot, J. Kröger, R. Berndt, A. Garcia-Lekue, W. A. Hofer, Atom transfer and single-adatom contacts. *Phys. Rev. Lett.* **94**, 126102 (2005).
37. G. Kresse, J. Furthmüller, Efficient iterative schemes for ab initio total-energy calculations using a plane-wave basis set. *Phys. Rev. B* **54**, 11169–11186 (1996).
38. J. P. Perdew, Y. Wang, Accurate and simple analytic representation of the electron-gas correlation energy. *Phys. Rev. B* **45**, 13244–13249 (1992).
39. B. Újfalussy, L. Szunyogh, P. Weinberger, Magnetism of 4*d* and 5*d* adlayers on Ag(001) and Au(001): Comparison between a nonrelativistic and a fully relativistic approach. *Phys. Rev. B* **51**, 12836–12839 (1995).
40. J. C. Slater, G. F. Koster, Simplified LCAO method for the periodic potential problem. *Phys. Rev.* **94**, 1498–1524 (1954).

41. J. Li, H. Chen, I. K. Drozdov, A. Yazdani, B. Andrei Bernevig, A. H. MacDonald, Topological superconductivity induced by ferromagnetic metal chains. *Phys. Rev. B* **90**, 235433 (2014).
42. D. A. Papaconstantopoulos, *Handbook of the Band Structure of Elemental Solids* (Springer, 2015).
43. B. Braunecker, G. I. Japaridze, J. Klinovaja, D. Loss, Spin-selective Peierls transition in interacting one-dimensional conductors with spin-orbit interaction. *Phys. Rev. B* **82**, 45127 (2010).
44. A. Kitaev, Periodic table for topological insulators and superconductors. *AIP Conf. Proc.* **1134**, 22 (2009).
45. S. Ryu, A. P. Schnyder, A. Furusaki, A. W. W. Ludwig, Topological insulators and superconductors: Tenfold way and dimensional hierarchy. *New J. Phys.* **12**, 065010 (2010).
46. A. Y. Kitaev, Unpaired Majorana fermions in quantum wires. *Phys.-Usp.* **44**, 131–136 (2001).

Acknowledgments: We thank A. Lászlóffy and L. Udvardi for their contributions to the ab initio calculations as well as D. Morr and his team for helpful discussions. **Funding:** This work was supported by the European Research Council (project no. 338802); the Deutsche Forschungsgemeinschaft via SFB668; the Alexander von Humboldt Foundation; the National Research, Development and Innovation Office of Hungary (project nos. K115575 and FK124100); the Slovak Academy of Sciences via the SASPRO Fellowship (project no. 1239/02/01); and the Tempus Foundation via the Hungarian State Eötvös Fellowship. **Author contributions:** H.K. and R.W. conceived and designed the experiments. H.K. and A.P.-M. carried out the experiments and analyzed the data. T.P. performed the tight-binding model and topological phase diagram calculations and discussed the results with L.R. and M.T. K.P. and L.S. determined the ab initio parameters used in the tight-binding model. R.W. supervised the project. H.K., T.P., L.R., and R.W. wrote the manuscript. All authors discussed the results and contributed to the manuscript. **Competing interests:** The authors declare that they have no competing interests. **Data and materials availability:** All data needed to evaluate the conclusions in the paper are present in the paper and/or the Supplementary Materials. Additional data related to this paper may be requested from the authors.

Submitted 17 November 2017
Accepted 23 March 2018
Published 11 May 2018
10.1126/sciadv.aar5251

Citation: H. Kim, A. Palacio-Morales, T. Posske, L. Rózsa, K. Palotás, L. Szunyogh, M. Thorwart, R. Wiesendanger, Toward tailoring Majorana bound states in artificially constructed magnetic atom chains on elemental superconductors. *Sci. Adv.* **4**, eaar5251 (2018).

Toward tailoring Majorana bound states in artificially constructed magnetic atom chains on elemental superconductors

Howon Kim, Alexandra Palacio-Morales, Thore Posske, Levente Rózsa, Krisztián Palotás, László Szunyogh, Michael Thorwart and Roland Wiesendanger

Sci Adv **4** (5), eaar5251.
DOI: 10.1126/sciadv.aar5251

Science Advances

AAAS

advances.sciencemag.org/cgi/content/full/4/5/eaar5251/DC1

Supplementary Materials for

Toward tailoring Majorana bound states in artificially constructed magnetic atom chains on elemental superconductors

Howon Kim, Alexandra Palacio-Morales, Thore Posske, Levente Rózsa, Krisztián Palotás, László Szunyogh, Michael Thorwart, Roland Wiesendanger

Published 11 May 2018, *Sci. Adv.* **4**, eaar5251 (2018)
DOI: 10.1126/sciadv.aar5251

The PDF file includes:

Other Supplementary Material for this manuscript includes the following:
(available at advances.sciencemag.org/cgi/content/full/4/5/eaar5251/DC1)

- movie S1 (.mp4 format). Demonstration of subsequent atom manipulations to construct the close-packed chains of various lengths.
- movie S2 (.mp4 format). Spatially resolved 2D spectroscopic maps for two different ends of the 40-atom-long Fe chain below T_C.
- movie S3 (.mp4 format). Spatially resolved 2D spectroscopic maps for the 40-atom-long Fe chain above T_C.

Supplementary Text

section S1. Ab initio calculations

The system-specific parameters for the tight-binding model calculations displayed in Fig. 4C were obtained in several steps. First, the energetically favored geometries of the Fe atomic structures on the Re(0001) surface have been determined by employing the Vienna Ab-initio Simulation Package (VASP) (*37*). During the calculations the generalized gradient approximation (GGA) in the Perdew–Wang 91 parametrization (PW91) (*38*) of the exchange-correlation functional within density functional theory (DFT) was used. The system was modelled as a 7×7 surface cell in order to avoid interaction of Fe atoms in repetitive supercells, in a slab geometry consisting of four layers of Re (in total $4\times7\times7=196$ Re atoms). The Re atoms in the bottom three layers have been fixed in their hcp bulk positions (in-plane lattice constant of 2.761 Å), and the topmost Re layer and the Fe atomic structures above have been relaxed. A vacuum region of minimum 9 Å thickness has been considered to avoid interaction between repetitive slabs. Due to the large size of the supercell, the Brillouin zone was sampled by the Gamma point only. It was found that the Fe adatom in the hcp hollow site is located closer to the top Re layer (1.84 Å) than the ideal interlayer distance in bulk Re (2.23 Å) due to its small size, and that it displays a stable spin magnetic moment of about $2.86\,\mu_B$. For investigating the geometry of an atomic chain, we considered a 4-atom-long Fe chain, where the Fe atoms reside in neighboring hcp hollow sites. After geometry optimization, we obtained very similar Fe-Re vertical distances of 1.85 and 1.87 Å and spin moments of 2.49 and $2.43\,\mu_B$ for the symmetrically distinct Fe atoms in the chain (outer and inner, respectively) as for the adatom case. Due to this similarity, we determined the tight-binding model parameters from calculations performed for the adatom case.

section S2. Model parameters

The on-site energy for the *d* electrons μ, the spin-splitting parameter J and the spin–orbit coupling strength λ used in the tight-binding model calculations were derived by investigating the resonance energies ε_n of the single-site potentials obtained self-consistently from SKKR and the Embedded Cluster methods (*39*). These resonance energies are associated with the eigenvalues of the effective one-electron Hamiltonian

$$H=\mu\boldsymbol{c}^{\dagger}\boldsymbol{c}+\boldsymbol{c}^{\dagger}(L_0\otimes JS^{Z})\boldsymbol{c}+\lambda\boldsymbol{c}^{\dagger}(\boldsymbol{LS})\boldsymbol{c} \qquad (1)$$

where $\boldsymbol{c}$ denotes the electron annihilation operators in the *d* states, $\boldsymbol{S}$ is the operator of the one-half spin of electrons, $\boldsymbol{L}$ stands for the angular momentum operator restricted to the *d* $(l=2)$ states, L_0 denotes the unit matrix in the same subspace, and $\boldsymbol{LS}=L^x\otimes S^x+L^y\otimes S^y+L^z\otimes S^z$. Note that in the Hamiltonian given by Eq. (1) we supposed that the exchange field is oriented along the *z* axis; however, this choice does not influence the eigenvalues. The on-site energy μ is given on a scale where the Fermi energy of the Re substrate corresponds to zero.

The parameters for the tight-binding model were determined from the self-consistent calculations performed for the Fe adatom. The resonance energies of the Fe potential showed basically a double-split, the two branches displaying five lines with almost equidistant separation. This situation typically corresponds to the case of large spin splitting (J) and small spin–orbit coupling (λ) as also discussed in ref. (*39*). Expanding perturbatively up to first order in λ, the eigenvalues

of H can be written as $\varepsilon_{m_l}^{\pm} = \mu \pm \frac{J}{2} \pm \frac{\lambda}{2} m_l$, $\pm$ denoting to the up- and down-spins and m_l =–2, –1, 0, 1, 2. This procedure led to the parameter values μ =–0.92 eV, J =2.18 eV and λ =0.06 eV.

section S3. Tight-binding model

In order to deduce the topological character of the electronic phase, we implemented a Slater–Koster tight-binding model (*40*, *41*) for the linear Fe chain. Our model is material-specific, based on the experimentally determined superconducting gap, the parameter values determined from *ab initio* calculations discussed above and hopping parameters from ref. (*42*). The Hamiltonian of the system reads

$$H = \sum_{\boldsymbol{r}} \mu \boldsymbol{c}_{\boldsymbol{r}}^{\dagger} \boldsymbol{c}_{\boldsymbol{r}} + \sum_{\boldsymbol{r},\delta\boldsymbol{r}} \boldsymbol{c}_{\boldsymbol{r}+\delta\boldsymbol{r}}^{\dagger} T(\delta\boldsymbol{r}) \boldsymbol{c}_{\boldsymbol{r}} + \lambda \sum_{\boldsymbol{r}} \boldsymbol{c}_{\boldsymbol{r}}^{\dagger} (\boldsymbol{L}\boldsymbol{S}) \boldsymbol{c}_{\boldsymbol{r}} + \sum_{\boldsymbol{r}} \boldsymbol{c}_{\boldsymbol{r}}^{\dagger} (L_0 \otimes J\boldsymbol{m}(\boldsymbol{r})\boldsymbol{S}) \boldsymbol{c}_{\boldsymbol{r}} + \left(\sum_{\boldsymbol{r}} \Delta \boldsymbol{c}_{\boldsymbol{r}}^{\dagger} (L_0 \otimes i\sigma^y) \boldsymbol{c}_{\boldsymbol{r}}^{\dagger} + h.c. \right) \quad (2)$$

Similarly to Eq. (1), $\boldsymbol{c}_{\boldsymbol{r}}$ are vectors containing the annihilation operators of the electrons in the *d* orbitals. The sums in $\boldsymbol{r}$ and $\delta\boldsymbol{r}$ run over the positions of the Fe atoms in the chain and the nearest-neighbor vectors, respectively. The coefficients μ, T, λ, J and Δ describe on-site energies, hopping matrices, spin–orbit coupling, spin splitting and superconducting pairing potential, respectively. The spin $\boldsymbol{S} = \frac{1}{2}(\sigma^x, \sigma^y, \sigma^z)$ is expressed by the Pauli matrices, the standard two-dimensional generators of *SU(2)*. The orbital moment $\boldsymbol{L}$ is given on the five-dimensional basis of the orbitals by the following representation of *SO(3)*

$$L_1 = i \begin{pmatrix} 0 & 0 & 1 & 0 & 0 \\ 0 & 0 & 0 & 1 & \sqrt{3} \\ -1 & 0 & 0 & 0 & 0 \\ 0 & -1 & 0 & 0 & 0 \\ 0 & -\sqrt{3} & 0 & 0 & 0 \end{pmatrix} \quad (3)$$

$$L_2 = i \begin{pmatrix} 0 & 1 & 0 & 0 & 0 \\ -1 & 0 & 0 & 0 & 0 \\ 0 & 0 & 0 & -1 & \sqrt{3} \\ 0 & 0 & 1 & 0 & 0 \\ 0 & 0 & -\sqrt{3} & 0 & 0 \end{pmatrix} \quad (4)$$

$$L_3 = i\begin{pmatrix} 0 & 0 & 0 & -2 & 0 \\ 0 & 0 & -1 & 0 & 0 \\ 0 & 1 & 0 & 0 & 0 \\ 2 & 0 & 0 & 0 & 0 \\ 0 & 0 & 0 & 0 & 0 \end{pmatrix} \quad (5)$$

These operators are expressed in the real basis xy, yz, zx, $x^2 - y^2$, $3z^2 - r^2$ of the orbital angular momentum.

The non-collinear magnetization of the chain is encoded in $\boldsymbol{m}(\boldsymbol{r})$. Since the experimental data suggest a modulation of both the in-plane and out-of-plane magnetization components with a period of $4\,a_{\mathrm{Re}}$ (see fig. S2), we considered a spin spiral rotating in the plane defined by the Fe chain and the out-of-plane direction with an angle of 90° between adjacent atoms. The choice of the rotational plane is also supported by symmetry considerations, which prefer this type of so-called cycloidal spin spiral states in surface magnetic structures due to the presence of the Dzyaloshinsky–Moriya interaction (*29*). As demonstrated in ref. (*43*), the non-collinear magnetic structure is equivalent to a ferromagnetic chain with an additional Rashba term, and this latter model was investigated in earlier publications (*41*).

The hopping matrices T between neighboring atoms mix the *d* orbitals (*40*), being of the form

$$T(\delta\boldsymbol{r}) = \sum_\alpha V^{dd\alpha}(|\delta\boldsymbol{r}|)E^{dd\alpha}(\delta\boldsymbol{r}/|\delta\boldsymbol{r}|) \otimes \sigma_0 \quad (6)$$

where α runs over σ, π and δ orbitals. Here, $V^{dd\alpha}$ are Slater–Koster two-center parameters in orthogonal basis and $E^{dd\alpha}$ are Slater–Koster matrices (*40*, *42*). The parameter-specific integrals $V^{dd\alpha}$ are derived from the Fe bulk values given in ref. (*42*) by scaling in order to account for the different lattice spacing that the Fe atoms assume on the Re surface. The expression for the scaling reads $V^{dd\alpha} = (a_{\mathrm{Re}}/a_{\mathrm{Fe}})^{-n^\alpha} V^{dd\alpha}_{\mathrm{Fe\,bulk}}$, with a_{Re} =2.761 Å the in-plane lattice constant of the hcp Re substrate, a_{Fe} =2.477 Å the distance between nearest neighbors in bulk bcc Fe, and the exponents $n^\sigma = 3$ and $n^\pi = n^\delta = 4$ (see ref. (*41*)). The rescaled parameters used for the calculations are $V^{dd\sigma} = -0.48$ eV, $V^{dd\pi} = 0.26$ eV and $V^{dd\delta} = -0.02$ eV. The effect of the Re surface is included in the proximity-induced superconductivity term $\Delta = 0.28$ meV, which was determined experimentally.

The Hamiltonian given by Eq. (2) is not time-reversal symmetric and it is classified by a $\mathbb{Z}_2$ topological invariant (*44*), being in the symmetry class with Cartan label *D* according to the classification in ref. (*45*). This invariant, called Majorana number, is given by (*46*)

$$\mathcal{M} = \mathrm{sgn}\left(Pf\left(\tilde{\mathrm{B}}(0)\right)Pf\left(\tilde{\mathrm{B}}(\pi)\right)\right) \tag{7}$$

where Pf denotes the Pfaffian of an antisymmetric matrix and $\tilde{\mathrm{B}}$ is the Fourier transform of the matrix B defined such that

$$\mathcal{H} = \sum_{\mathbf{r}_1,\mathbf{r}_2} \boldsymbol{\gamma}_{\mathbf{r}_2}^T B(\mathbf{r}_2 - \mathbf{r}_1)\boldsymbol{\gamma}_{\mathbf{r}_1} \tag{8}$$

with $\boldsymbol{\gamma}_{\mathbf{r}} = (\gamma_{\mathbf{r},i,l,s})_{i\in(1,2),l\in(-2,-1,0,1,2),s\in(\uparrow,\downarrow)}$ being a vector containing the Majorana operators

$$\begin{aligned}\gamma_{\mathbf{r},1,l,s} &= c^{\dagger}_{\mathbf{r},l,s} + c_{\mathbf{r},l,s} \\ \gamma_{\mathbf{r},2,l,s} &= i(c^{\dagger}_{\mathbf{r},l,s} - c_{\mathbf{r},l,s})\end{aligned} \tag{9}$$

with the l and s indices describing the angular momentum and spin quantum numbers. The Majorana number in Eq. (7) takes the value of $\mathcal{M} = 1$ in the topologically trivial and $\mathcal{M} = -1$ in the topologically non-trivial phase, shown in Fig. 4C.

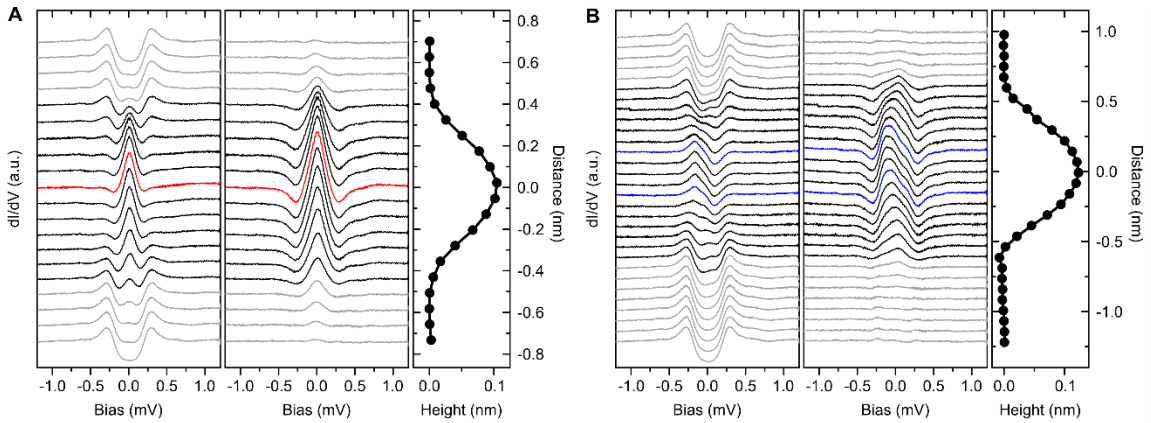

fig. S1. Spatial distribution of the YSR states for a single Fe atom and an Fe dimer on the Re(0001) surface. (**A** and **B**) Spatially-resolved dI/dV spectra across (A) a single Fe atom and (B) an Fe dimer. The raw spectra are presented at the left, the spectra after subtracting the spectrum on the bare Re substrate in the middle, and the corresponding surface profile on the right. The dots indicate the locations where the spectra were obtained. The spectra obtained within atomic protrusions in the topographic profiles are plotted in black for both panels, while grey denotes spectra obtained above the Re substrate. The spectra taken just above the Fe atoms are depicted in red for the single Fe atom and in blue for the Fe dimer in panels (A) and (B), respectively. For both the single atom and the dimer, the intensity of the YSR peak decays within a few atomic lattice constants (~1 nm) inside the Re substrate, with spatial variations of the spectral shape.

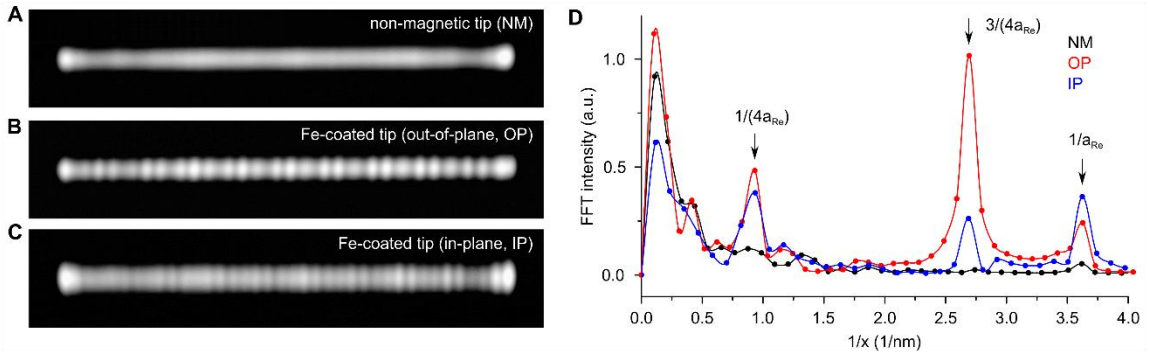

fig. S2. The fast Fourier transformation analysis for the magnetic structure of the 40-atom-long Fe chain. (**A**)-(**C**) Contrast-adjusted (SP)-STM images measured with (A) a non-magnetic PtIr tip and Fe-coated tips sensitive to (B) the out-of-plane and (C) the in-plane component of the magnetization along the chain. The (SP)-STM data are identical to the ones displayed in Figs. 2C-E. (**D**) FFT analysis plot for determining the period of the modulations observed in the (SP)-STM profiles with the three different tips. There are two dominant periodic modulations, $4\,a_{\mathrm{Re}}$ ~1.1 nm and $4/3\,a_{\mathrm{Re}}$ ~0.36 nm, which are visible in the FFT spectra obtained with both spin-sensitive Fe coated tips, but are absent for the one taken with the non-magnetic tip. The contribution of the atomic corrugation in the Fe chain appears at $1/a_{\mathrm{Re}}$ in all three FFT spectra.

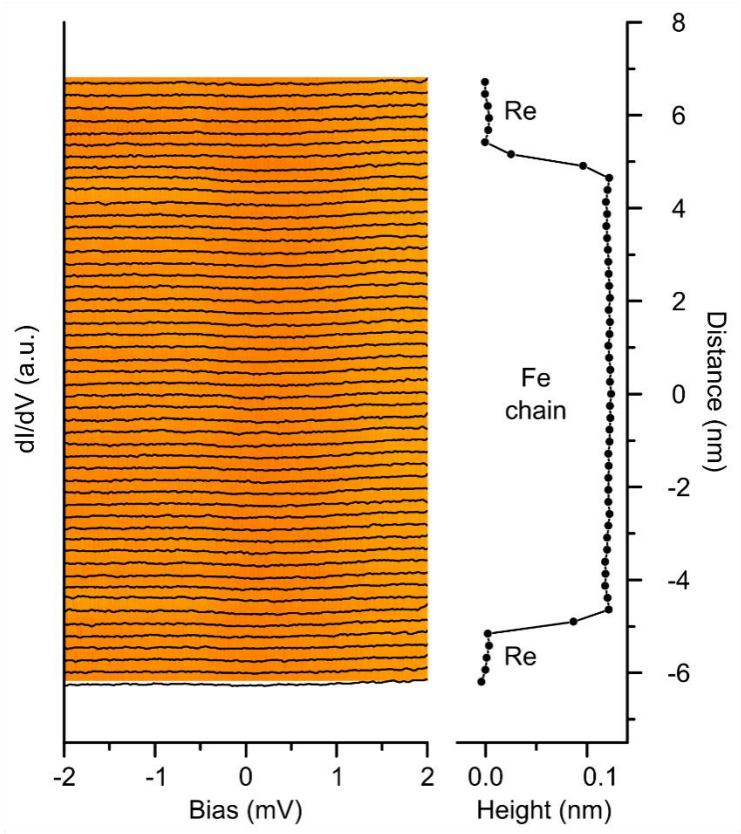

fig. S3. Absence of the in-gap states on the 40-atom-long Fe chain above the superconducting critical temperature of Re. (left) Spatially-resolved dI/dV spectra and colour-coded spectroscopic map along the chain taken at a temperature above the superconducting critical temperature of the Re (T=1.7 K, tunneling parameters I_T=5.0 nA, V_S=3.0 mV). The spectra taken on both the Re substrate and the Fe chain display a featureless almost constant LDOS at the Fermi energy. This indicates that superconductivity of the Re substrate is fully suppressed and all in-gap features on the Fe chain have disappeared. (right) Simultaneously obtained topographic profile during the spectroscopic measurement. The dots indicate the spatial positions where the spectra were obtained.

movie S1. Demonstration of subsequent atom manipulations to construct the close-packed chains of various lengths.

movie S2. Spatially resolved 2D spectroscopic maps for two different ends of the 40-atom-long Fe chain below T_C.

movie S3. Spatially resolved 2D spectroscopic maps for the 40-atom-long Fe chain above T_C.